Dynamic Mode Decomposition Applied to the Study of a High Reynolds Number Supersonic Jet Flow

Sami Yamouni, sami.yamouni@gmail.com[1]
Carlos Junqueira-Junior, junior.hmg@gmail.com[1]
João Luiz F. Azevedo, joaoluiz.azevedo@gmail.com[2]
William R. Wolf, wolf@fem.unicamp.br[3]

[1] Instituto Tecnológico de Aeronáutica, São José dos Campos, SP, Brazil
[2] Instituto de Aeronáutica e Espaço, São José dos Campos, SP, Brazil
[3] Universidade Estadual de Campinas, Campinas, SP, Brazil

Abstract: *Current design constraints have encouraged the studies of aeroacoustic fields around compressible jet flows. The present work addresses the numerical study of turbulence modeling of unsteady turbulent jet flows for aeroacoustic analyses of main engine rocket plumes. A novel large eddy simulation (LES) tool has been developed in order to reproduce high fidelity results of compressible jet flows which could be used for aeroacoustic studies with the Ffowcs Williams and Hawkings approach. The large eddy simulation formulation is written using the finite difference approach. The energy equation is carefully discretized in order to model the energy equation of the filtered Navier-Stokes formulation. The classical Smagorinsky model is the subgrid scale closure selected for the present work. Numerical simulations of perfectly expanded jets are performed and the results are compared with the literature in order to validate the present implementation. Morever, dynamic mode decomposition (DMD) is applied to identify the contribution of the structures associated to a single frequency on the acoustic directivity. Finally, the jet flow dynamics is described using the most relevant DMD modes, and compared with the unsteady flow results obtained previously.*

Keywords: *LES, Supersonic Jets, DMD, CFD*

1. INTRODUCTION

One of the main design issues related to launch vehicles lies on noise emission originated by the complex interaction between the high-temperature/high-velocity exhaustion gases and the atmospheric air. These emissions, which have high noise levels, can damage the launching structure or even be reflected upon the vehicle structure itself and the equipment onboard at the top of the vehicles. Moreover, the resulting pressure fluctuations can damage the solid structure of different parts of the launcher or the onboard scientific equipment by vibrational acoustic stress. Therefore, it is strongly recommended to consider the load resulted from acoustic sources over large launching vehicles during take-off and also during the transonic flight. Moreover, one cannot neglect the energy dissipation effect generated by the acoustic waves even if the vehicle is far from the ground. Theoretically, all chemical energy should be converted to kinetic energy. However, in reality, the noise generation consumes part of the chemical energy.

The acoustics design constraints have encouraged the studies of aeroacoustic fields around compressible jet flows. Instituto de Aeronautica e Espaço (IAE), in Brazil, is interested in this flow configuration for rocket design applications. Unsteady property fields of the flow are necessary for the aerocoustic study. Therefore, the present work addresses the numerical study of unsteady turbulent compressible jet flows for such aeroacoustic applications. A new computational tool is developed regarding the study of unsteady turbulent compressible flow. The novel large eddy simulation (LES) tool is developed in order to reproduce high fidelity results of compressible jet flows which are used for aeroacoustic studies using the Ffowcs Williams and Hawkings approach (Wolf and Lele, 2011).

Finally, with the objective of simplifying a complex flow into a low-dimensional representation containing the dominant dynamic structures, different techniques have been proposed. Among them, the Proper Orthogonal Decomposition (POD) (Lumley, 1970; Sirovich, 1987; Berkooz *et al.*, 1993), and the Dynamic mode Decomposition (DMD) (Schmid, 2010) are the more commonly used in the fluid community. The POD selects the modes depending on their energy contents. However, this criterion is not necessarily correct since the energy is not always the key parameter to identify the flow structures (Schmid, 2010). In contrast with the POD, the modes computed from the DMD define characteristic frequencies of the flow. This is the chosen method in the present work. DMD has already been applied to various flow configurations such as cavity flows (Schmid, 2010; Seena and Sung, 2011), shockwave-turbulent boundary layer interaction (Grilli *et al.*, 2012), boundary layer flows (Sayadi *et al.*, 2013; Tang and Jiang, 2012), cylinder flows (Bagheri, 2013; Tissot *et al.*, 2013), combustion chamber flow (Jourdain *et al.*, 2013; Abou-Taouk *et al.*, 2015), wake behind a flexible membrane (Schmid, 2010) or jet flows (Lárusson *et al.*, 2014; Schmid, 2011; Schmid *et al.*, 2011, 2012; Stegeman *et al.*, 2014; Wan *et al.*, 2015). And several variations of the DMD algorithm have also been proposed. One can cite the optimal mode decomposition (Wynn *et al.*, 2013), the sparsity-promoting DMD (Jovanović *et al.*, 2014), the extended DMD (Williams *et al.*, 2014, 2015), or the streaming DMD (Hemati *et al.*, 2014). Lately, an unbiased noise-robust method has been proposed by Hemati and Rowley (2015) to overcome the adverse influence of measurment errors. This method can be combined with all the DMD algorithm listed above.

The objective of the present work is to apply the DMD algorithm to the numerical data extracted from a large eddy simulation of a perfectly-expanded supersonic jet flow at $M = 1.4$. Due to the large dimension of this problem, the author will use the streaming version (Hemati *et al.*, 2014) of the *total-least square* DMD formulation proposed by Hemati and Rowley (2015). Finally, preliminary DMD results will be displayed and compared with the unsteady LES results.

2. NAVIER-STOKES EQUATIONS

The numerical strategy used in the present study is based on the compressible Navier-Stokes equations formulated as

$$\frac{\partial \rho}{\partial t} + \frac{\partial}{\partial x_j}\left(\rho u_j\right) = 0\,, \tag{1}$$

$$\frac{\partial}{\partial t}\left(\rho u_i\right) + \frac{\partial}{\partial x_j}\left(\rho u_i u_j\right) + \frac{\partial p}{\partial x_i} - \frac{\partial \tau_{ij}}{\partial x_j} = 0\,, \tag{2}$$

$$\frac{\partial e}{\partial t} + \frac{\partial}{\partial x_j}\left[\left(e + p\right) u_j - \tau_{ij} u_i + q_j\right] = 0\,, \tag{3}$$

in which t and x_i are independent variables representing time and spatial coordinates of a Cartesian coordinate system $\mathbf{x}$, respectively. The components of the velocity vector $\mathbf{u}$ are written as u_i, and $i = 1, 2, 3$. Density, pressure and total energy per mass unit are denoted by ρ, p and e, respectively. The heat flux vector, q_j, is given by

$$q_j = \kappa \frac{\partial T}{\partial x_j}\,, \tag{4}$$

where T is the static temperature and κ is the thermal conductivity coefficient, which can by expressed by

$$\kappa = \frac{\mu C_p}{Pr}\ . \tag{5}$$

The thermal conductivity coefficient is a function of the specific heat at constant pressure, C_p, of the Prandtl number, Pr, which is equal to 0.72 for air, and of the dynamic viscosity coefficient, μ. The latter can be calculated using Sutherland's law,

$$\mu\left(T\right) = \mu_\infty \left(\frac{T}{T_\infty}\right)^{\frac{3}{2}} \frac{T_0 + S_1}{T + S_1}\,, \qquad \text{with } S_1 = 110.4 \text{ K}\,. \tag{6}$$

According to the Stokes hypothesis, the shear-stress tensor, τ_{ij}, for a Newtonian fluid can be written as

$$\tau_{ij} = 2\mu\left(S_{ij} - \frac{1}{3}\delta_{ij} S_{kk}\right)\,, \tag{7}$$

in which the components of rate-of-strain tensor, S_{ij}, are given by

$$S_{ij} = \frac{1}{2}\left(\frac{\partial u_i}{\partial x_j} + \frac{\partial u_j}{\partial x_i}\right)\,. \tag{8}$$

In order to close the system of equations the density, the static pressure and the static temperature are correlated by the equation of state given by

$$p = \rho R T\,, \tag{9}$$

where R is the gas constant, written as

$$R = C_p - C_v\,, \tag{10}$$

and C_v is the specif heat at constant volume. The total energy per mass unity is given by:

$$e = \frac{p}{\gamma - 1} + \frac{1}{2}\rho u_i u_i\,, \tag{11}$$

in which γ is the ratio of specific heats, written as $\gamma = C_p / C_v$.

3. LARGE EDDY SIMULATION FILTERING

The large eddy simulation is based on the principle of scale separation, which is addressed as a filtering procedure in a mathematical formalism. A modified version of the the System I filtering approach (Vreman, 1995) is used in present

work. The resulting filtered formulation is written as

$$\begin{gathered}
\frac{\partial \overline{\rho}}{\partial t} + \frac{\partial}{\partial x_j}\left(\overline{\rho}\widetilde{u_j}\right) = 0\,, \\
\frac{\partial}{\partial t}\left(\overline{\rho}\widetilde{u_i}\right) + \frac{\partial}{\partial x_j}\left(\overline{\rho}\widetilde{u_i}\widetilde{u_j}\right) + \frac{\partial \overline{p}}{\partial x_i} - \frac{\partial \tau_{ij}^{mod}}{\partial x_j} + \frac{1}{3}\frac{\partial}{\partial x_j}\left(\delta_{ij}\sigma_{ii}\right) = 0\,, \\
\frac{\partial \check{e}}{\partial t} + \frac{\partial}{\partial x_j}\left[\left(\check{e} + \overline{p}\right)\widetilde{u_j}\right] - \frac{\partial}{\partial x_j}\left(\tau_{ij}^{mod}\widetilde{u_i}\right) + \frac{1}{3}\frac{\partial}{\partial x_j}\left[\left(\delta_{ij}\sigma_{ii}\right)\widetilde{u_i}\right] + \frac{\partial q_j^{mod}}{\partial x_j} = 0\,,
\end{gathered} \tag{12}$$

where, τ_{ij}^{mod} and q_j^{mod}, include the viscous and the subgrid terms. They can be written as

$$\tau_{ij}^{mod} = 2\left(\mu + \mu_{sgs}\right)\left(S_{ij} - \frac{1}{3}\delta_{ij}S_{kk}\right) \tag{13}$$

and

$$q_j^{mod} = \left(\kappa + \kappa_{sgs}\right)\frac{\partial T}{\partial x_j}\,. \tag{14}$$

4. SUBGRID SCALE CLOSURE

This section describes the subgrid scale closure included in the present work, the Smagorinsky model. The Smagorinsky model (Smagorinsky, 1963) is one of the simplest algebric models for the deviatory part of the SGS stress tensor used in large eddy simulations. The isotropic part of the stress SGS tensor is neglected for the Smagorinsky model in the current work. This SGS closure is a classical model based on the large scales properties. It became very famous with the work of Deardorff (1970) and Lilly (1965). It is generally used in a local form of the physical space in order to be more adaptable to the flow being calculated. It is obtained by space and time localization of statistical relations. There is no particular justification for this local use of relations that are on the average true for the whole, since they only ensure that the energy transfer through the cutoff are expressed on the average, and not locally (Sagaut, 2002). The Smagorinsky model is written as

$$\mu_{sgs} = \left(\rho C_s \Delta\right)^2 |\check{S}|\,, \tag{15}$$

where

$$|\check{S}| = \left(2\check{S}_{ij}\check{S}_{ij}\right)^{\frac{1}{2}}\,, \tag{16}$$

and C_s is the Smagorinsky constant. Several attempts can be found in the literature regarding the evaluation of the Smagorinsky constant. The value of this constant is adjusted to improve the results of different flow configurations. Using the eddy-damped quasi-normal Markovian theory (EDQNM), one can find $C_s = 0.148$ (Sagaut, 2002; Aupoix and Cousteix, 1982). Lilly work suggests $C_s = 0.18$ (Lilly, 1967). Clark *et al.* (1979), for isotropic homogeneous turbulence, use $C_s = 0.2$. Deardorff (1970) uses $C_s = 0.1$ for a plane channel flow. Studies performed using experimental data yield $0.1 < C_s < 0.12$ (Meneveau, 1994; Ulitsky and Collins, 2000; O'Neil and Meneveau, 1997). Finite Reynolds number and spectrum shape can be taken into account leading to a complex definition of C_s (Meyers and Sagaut, 2006). In pratical terms, the Smagorinsky subgrid model has a flow dependency of the constant which takes value ranging from 0.1 to 0.2 depending on the flow. The suggestion of Lilly, $C_s = 0.18$, is used in the current work.

This model is generally over-dissipative in regions of large mean strain. This is particularly true in the transitional region between laminar and turbulent flows. Moreover, the limiting behavior near the wall is not correct, and the model predictions correlate poorly with the exact subgrid scale tensor (Garnier *et al.*, 2009). However, it is a very simple model and, with the use of damping function and good calibration, it can be successfully applied in large eddy simulations.

5. NUMERICAL FORMULATION

The governing equations previously described are discretized in a structured finite difference context for general curvilinear coordinate system (Bigarella, 2002). The numerical flux is calculated through a central difference scheme with the explicit addition of the anisotropic scalar artificial dissipation of Turkel and Vatsa (1994). The time integration is performed by an explicit, 2nd-order, 5-stage Runge-Kutta scheme (Jameson and Mavriplis, 1986; Jameson *et al.*, 1981). Conserved properties and artificial dissipation terms are properly treated near boundaries in order to assure the physical correctness of the numerical formulation. The interested reader is referred to Refs. Junqueira-Junior *et al.* (2015b); Junqueira-Junior (2016) for additional details.

5.1 Spatial Discretization

For the remainder of the paper, the authors will drop all underbars and tildes in the formulation for the sake of simplicity. Nevertheless, the reader should be advised that all equations are referring to filtered dimensionless quantities

(Bigarella, 2002; Junqueira-Junior, 2016). The work uses a finite difference framework in order to discretize the governing equations. Hence, the result of the discretization of the spatial derivatives in the governing equations can be written as

$$\left(\frac{\partial Q}{\partial t}\right)_{i,j,k} = -RHS_{i,j,k} \ . \tag{17}$$

Here, $RHS_{i,j,k}$ represents the residue for the (i,j,k) grid point. It is very convenient to write $RHS_{i,j,k}$ as a function of the numerical flux vectors at the interfaces between grid points, following a nomenclature similar to the one used in Ref. Turkel and Vatsa (1994). Therefore, the residue can be written as

$$\begin{aligned} RHS_{i,j,k} &= \frac{1}{\Delta\xi}\left(\mathbf{E}_{e(i+\frac{1}{2},j,k)} - \mathbf{E}_{e(i-\frac{1}{2},j,k)} - \mathbf{E}_{v(i+\frac{1}{2},j,k)} + \mathbf{E}_{v(i-\frac{1}{2},j,k)}\right) \\ &\quad \frac{1}{\Delta\eta}\left(\mathbf{F}_{e(i,j+\frac{1}{2},k)} - \mathbf{F}_{e(i,j-\frac{1}{2},k)} - \mathbf{F}_{v(i,j+\frac{1}{2},k)} + \mathbf{F}_{v(i,j-\frac{1}{2},k)}\right) \\ &\quad \frac{1}{\Delta\zeta}\left(\mathbf{G}_{e(i,j,k+\frac{1}{2})} - \mathbf{G}_{e(i,j,k-\frac{1}{2})} - \mathbf{G}_{v(i,j,k+\frac{1}{2})} + \mathbf{G}_{v(i,j,k-\frac{1}{2})}\right) . \end{aligned} \tag{18}$$

Since a centered spatial discretization is being considered, the interface numerical flux vectors are defined as the arithmetic average of the corresponding physical flux vectors at the two grid points that share that interface. However, still due to the use of a centered scheme, the inviscid numerical fluxes must be augmented by artificial dissipation terms, in order to maintain numerical stability. In the present case, the scalar, non-isotropic, artificial dissipation model proposed by Turkel and Vatsa (1994) is used. Hence, the numerical inviscid interface fluxes are written as

$$\begin{aligned} \mathbf{E}_{e(i\pm\frac{1}{2},j,k)} &= \frac{1}{2}\left(\mathbf{E}_{e(i,j,k)} + \mathbf{E}_{e(i\pm1,j,k)}\right) - J^{-1}\mathbf{d}_{(i\pm\frac{1}{2},j,k)} , \\ \mathbf{F}_{e(i,j\pm\frac{1}{2},k)} &= \frac{1}{2}\left(\mathbf{F}_{e(i,j,k)} + \mathbf{F}_{e(i,j\pm1,k)}\right) - J^{-1}\mathbf{d}_{(i,j\pm\frac{1}{2},k)} , \\ \mathbf{G}_{e(i,j,k\pm\frac{1}{2})} &= \frac{1}{2}\left(\mathbf{G}_{e(i,j,k)} + \mathbf{G}_{e(i,j,k\pm1)}\right) - J^{-1}\mathbf{d}_{(i,j,k\pm\frac{1}{2})} , \end{aligned} \tag{19}$$

where the $\mathbf{d}_{(i\pm\frac{1}{2},j,k)}$, $\mathbf{d}_{(i,j\pm\frac{1}{2},k)}$ and $\mathbf{d}_{(i,j,k\pm\frac{1}{2})}$ terms are the artificial dissipation operators. For instance, the operator in the ξ direction, at the $(i+1/2)$ interface, can be expressed as

$$\begin{aligned} \mathbf{d}_{(i+\frac{1}{2},j,k)} &= \lambda_{(i+\frac{1}{2},j,k)}\left[\epsilon^{(2)}_{(i+\frac{1}{2},j,k)}\left(\mathcal{W}_{(i+1,j,k)} - \mathcal{W}_{(i,j,k)}\right)\right. \\ &\quad \left.\epsilon^{(4)}_{(i+\frac{1}{2},j,k)}\left(\mathcal{W}_{(i+2,j,k)} - 3\mathcal{W}_{(i+1,j,k)} + 3\mathcal{W}_{(i,j,k)} - \mathcal{W}_{(i-1,j,k)}\right)\right] . \end{aligned} \tag{20}$$

In this equation, the $\epsilon^{(2)}$ and $\epsilon^{(4)}$ are written as

$$\epsilon^{(2)}_{(i+\frac{1}{2},j,k)} = k^{(2)}\max\left(\nu^{d}_{(i+1,j,k)}, \nu^{d}_{(i,j,k)}\right) , \tag{21}$$

$$\epsilon^{(4)}_{(i+\frac{1}{2},j,k)} = \max\left[0, k^{(4)} - \epsilon^{(2)}_{(i+\frac{1}{2},j,k)}\right] . \tag{22}$$

The pressure gradient sensor operator, $\nu^{d}_{(i,j,k)}$, for the ξ direction is defined as

$$\nu^{d}_{(i,j,k)} = \frac{|p_{(i+1,j,k)} - 2p_{(i,j,k)} + p_{(i-1,j,k)}|}{p_{(i+1,j,k)} - 2p_{(i,j,k)} + p_{(i-1,j,k)}} . \tag{23}$$

It should be emphasized that the present artificial dissipation model is nonlinear and, hence, it allows for the selection between second and fourth difference artificial dissipation terms. Furthermore, the scaling of the artificial dissipation operator in each coordinate direction, for instance, $\lambda_{(i+\frac{1}{2},j,k)}$ in Eq. (20), is primarily weighted by its own spectral radius of the corresponding flux Jacobian matrix, which gives the non-isotropic characteristics to the model (Bigarella, 2002; Turkel and Vatsa, 1994).

Further details on the artificial dissipation model here adopted can be seen in the original paper by Turkel and Vatsa (1994) or in Refs. Bigarella (2002), Junqueira-Junior *et al.* (2015b) and Junqueira-Junior (2016). Computational aspects of the present implementation of the model and, in particular, issues associated to the computation of the various terms at partition interfaces, for parallel implementations, are discussed in detail in Refs. Junqueira-Junior *et al.* (2015b) and Junqueira-Junior (2016).

5.2 Time Marching Method

Since the present work is concerned with LES calculations, an explicit time marching method is adopted. Hence, the five-stage, second-order, explicit Runge-Kutta time stepping algorithm used in many aerospace solvers (Bigarella, 2002;

Jameson and Mavriplis, 1986; Jameson *et al.*, 1981) is also employed here. The time marching process can be expressed as

$$\begin{array}{lcll} Q^{(0)}_{(i,j,k)} & = & Q^{n}_{(i,j,k)}\,, & \\ Q^{(\ell)}_{(i,j,k)} & = & Q^{(0)}_{(i,j,k)} - & \alpha_\ell\,\Delta t\,RHS^{(\ell-1)}_{(i,j,k)} \qquad\qquad \ell = 1, 2 \cdots 5, \\ Q^{n+1}_{(i,jk,)} & = & Q^{(5)}_{(i,jk,)}\,, & \end{array} \tag{24}$$

The process of validation of the present solver has addressed the issues related to the use of an explicit time integration, and it has indicated that the above time marching scheme is sufficiently adequate for the current purposes. For further details in such studies, the interested reader is referred to Refs. Junqueira-Junior *et al.* (2015a) and Junqueira-Junior (2016). Clearly, in the previous equation, Δt is the time step, and n and $n+1$ indicate the property values at the current and at the next time step, respectively. The values adopted for the α_ℓ parameters are

$$\alpha_1 = \tfrac{1}{4} \quad , \qquad \alpha_2 = \tfrac{1}{6} \quad , \qquad \alpha_3 = \tfrac{3}{8} \quad , \qquad \alpha_4 = \tfrac{1}{2} \quad , \qquad \alpha_5 = 1 \ , \tag{25}$$

according to the original reference that presents this specific Runge-Kutta method (Jameson and Mavriplis, 1986). The time marching scheme is linearly stable for $CFL \leq 2\sqrt{2}$ (Bigarella, 2002).

5.3 Boundary Conditions

As in any application, the correct implementation of appropriate boundary conditions is a crucial step for successful simulations. In the present work, the overall geometry used for the computational domain has a cylindrical shape, which is obtained by the rotation of a 2-D plan around a centerline. Figure 1 presents a lateral view and a frontal view of the computational domain, indicating the position of the various types of boundary conditions which appear in the current test cases. Therefore, it is clear that the types of boundary conditions that must be addressed in the present work include entrance, exit, centerline, far field and periodic boundary conditions.

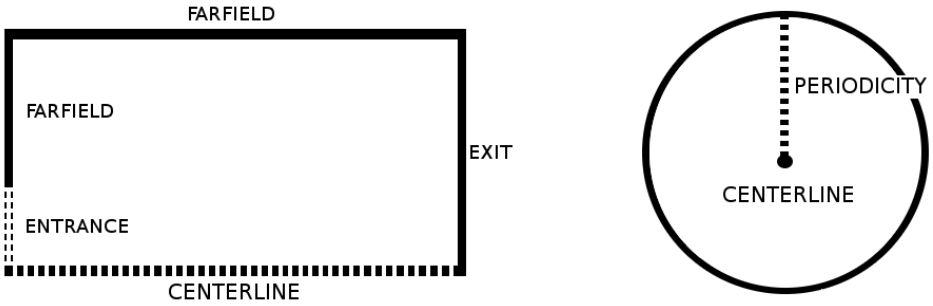

Figura 1: Lateral and frontal views of the computational domain indicating boundary conditions.

The implementation procedure adopted in the present work for each of these types of boundary conditions is described in detail in Ref. Junqueira-Junior *et al.* (2015b), and such a detailed presentation of the boundary condition enforcement procedure will not be repeated here. However, it is worth mentioning that far field conditions are addressed using the concept of Riemann invariants (Long *et al.*, 1991). The formulation of the entrance and exit boundary conditions uses the concept of the one-dimensional characteristic relations for the multi-dimensional Euler equations. Such an approach allows the definition of properties that must be provided at a given boundary and those that should be somehow extrapolated from interior information (Bigarella, 2002, 2007; Junqueira-Junior, 2016).

Of particular concern is the jet entrance boundary since, in principle, a fully turbulent jet should be entering the computational domain. In the present case, a simple flat-hat velocity profile, with the specified jet Mach number, is used at the entrance boundary. Further details and discussion of the effects of this selection are presented in the forthcoming sections of the paper. Finally, the centerline boundary is a singularity of the coordinate transformation and, hence, a careful treatment of this boundary is necessary. In the present approach, the conserved properties are extrapolated from the adjacent longitudinal plane and they are averaged in the azimuthal direction in order to define the updated properties at the centerline of the jet. The interested reader is referred to Refs. Junqueira-Junior *et al.* (2015b) and Junqueira-Junior (2016) for additional details of the boundary condition implementation.

6. DYNAMIC MODE DECOMPOSITION

6.1 Theoretical Framework

The DMD method provides a spatio-temporal decomposition of the flow into a set of dynamic modes that are derived from time-resolved snapshots. For example, the flow variable $\mathbf{x}_{DMD}(x, y, z, t)$, where x, y, z and t represent the spatial

coordinates and the time, respectively, can be represented by

$$\mathbf{x}_{DMD}(x,y,z,t) = \sum_{i=1}^{m-1} a_i exp(\lambda_i t)\phi_i(x,y,z), \tag{26}$$

where a_i and λ_i are the amplitude and the frequency of the spatial mode ϕ_i. The underlying mathematics is closely related to the idea of the Arnoldi algorithm (Schmid, 2010). This flow variable extracted from the simulation can be represented in the form of a snapshot sequence $X = [\mathbf{x}_1, \cdots, \mathbf{x}_m] \in \mathbb{R}^{n\times m}$, where $\mathbf{x}_i \in \mathbb{R}^n$ is the ith snapshot, m denotes the number of snapshots and n, the spatial dimension per time snapshot. In the present study, each snapshot $\mathbf{x}_i$ contains the whole set of conservative variables (ρ, ρU, ρV, ρW, e) but it depends on the user's choice. Even though recent techniques allow irregularly spaced sampling in time of the data (Tu *et al.*, 2014), the present study is designed to collect data regularly separated in time by Δt.

We assume that there exists a linear operator $\mathcal{A} \in \mathbb{R}^{n\times n}$ connecting two consecutive snapshot giving

$$\mathbf{x}_{i+1} = \mathcal{A}\mathbf{x}_i \quad \text{for } i = 1, \cdots, \mathrm{m}-1. \tag{27}$$

A is an approximation of the Koopman operator (Rowley *et al.*, 2009), whose eigen-elements can approximate the underlying dynamics of the flow, even non-linear. The objective of the DMD is the determination of these characteristics, such as the eigenvalues, the eigenvectors or the energy amplification, representing the flow dynamics. The selection of the eigen-elements of A is a matter of importance since the resulting reduced order model will directly depend on it. The classical strategy initially proposed by Schmid (2010) is described below. When the number of snapshots is increased, the flow is assumed to approach linear dependency. The m^{th} snapshot can then be expressed as a linear combination of the previous m-1 snapshots such as

$$\begin{aligned} \mathbf{x}_m &= c_1\mathbf{x}_1 + c_2\mathbf{x}_2 + \cdots + c_{m-1}\mathbf{x}_{m-1} + \epsilon \\ &= X_1^{m-1}\mathbf{c} + \epsilon. \end{aligned} \tag{28}$$

By using Eq. (27), this becomes

$$\mathcal{A}X_1^{m-1} = X_2^m = X_1^{m-1}C + \epsilon\mathbf{e}_{m-1}^T, \tag{29}$$

where ϵ is the residual, $\mathbf{e}$ is the i^{th} Euclidean unitary vector and $C \in \mathbb{R}^{(m-1)\times(m-1)}$ is the companion matrix defined as

Finally, it can be deduced from Eq. (29), knowing a couple of eigen-elements of C, (W_j,μ_j), that ($\phi_j = X_1^{m-1}W_j$, μ_j) is an approximation of the eigen-elements of A.

A discretized version of Eq. (26) expressed at any time instant $k = 1, \cdots, m-1$ is given as

$$\mathbf{x}_k = \sum_{i=1}^{m-1} \theta_i(k)\phi_i, \tag{31}$$

where θ_i are the temporal coefficient of the eigenvectors ϕ_i. Using Eq. (27), it comes directly that

$$\begin{aligned} \mathbf{x}_{k+1} &= \mathcal{A}\mathbf{x}_k = \sum_{i=1}^{m-1} \theta_i(k)\mathcal{A}\phi_i = \sum_{i=1}^{m-1} \theta_i(k)\mu_i\phi_i \\ &= \mathcal{A}^k\mathbf{x}_1 = \sum_{i=1}^{m-1} \theta_i(1)\mu_i^k\phi_i, \end{aligned} \tag{32}$$

and the associated growth rate and frequency of the i^{th} DMD mode of the complex frequency of Eq. (26) can be expressed as a function of the eigenvalue of A as,

$$\lambda_i = \frac{\log(\mu_i)}{\Delta t} \quad \text{with} \quad \sigma_i = \frac{\log(|\mu_i|)}{\Delta t} \quad \text{and} \quad \omega_i = \frac{\arg(\mu_i)}{\Delta t}\,. \tag{33}$$

In the present work, due to the large dimension of the problem, an alternative procedure, the streaming version (Hemati *et al.*, 2014) of the *Total-Least-Square* DMD algorithm (Hemati and Rowley, 2015) will be used. Formulation details are given by Hemati *et al.* (2014). This procedure allows an incremental update of new available snapshots, without storing all of them in memory. Therefore, the DMD routine is running in parallel of the CFD software, waiting for new snapshots to update its basis.

6.2 Choice of the Parameters

Two main parameters are considered in the DMD framework initially introduced by Schmid (2010). The first one is Δt, the constant time-step between two consecutive snapshots, while the second one is m, the total number of snapshots. Both of them require a good knowledge of the physical phenomenon under study. According to Schmid (2010), the sample rate must be sufficiently high, about three times the Nyquist cutoff, to capture correctly the dynamics of an oscillatory flow. The idea is then to tune the sampling frequency based on the phenomenon the user wants to study. However, following Chen *et al.* (2012), when using a high sample rate, the snapshots are likely to be correlated in time. This is a problem since the method impose the use of a linear independent dataset to work properly. In the algorithm used in the present work, a Gram-Schmidt step is included in the process to address this problem (Hemati *et al.*, 2014; Tissot *et al.*, 2013).

7. MESH GENERATION

A structured mesh generator is created in order to provide CGNS grid files for the simulations performed in the present work. Figure 2(a) illustrates a 3-D view of the two computational domains used in the current work. The geometry is colored by a time solution of the axial component of velocity of the flow. The complete 3-D mesh is created by rotating a 2-D mesh around the horizontal direction, x. A slice in the radial direction of the 3-D mesh is illustrated in Fig. 2(b). The rotation approach generates a singularity at the centerline of the domain. The treatment of this region is discussed in the boundary conditions section. The authors chose not to include the nozzle geometry and the jet entrance is located at $x = 0$, between $|r|/D \leq 0.5$, where $|r|$ is the distance from the centerline in the radial direction and D is the incoming jet diameter. The refinement is performed using hyperbolic tangent functions, with a finest grid resolution near the jet entrance and along the slip line of the jet. The mesh is coarsened in the far field in order to diffuse the acoustic waves and avoid reflections at the farfield domain boundaries.

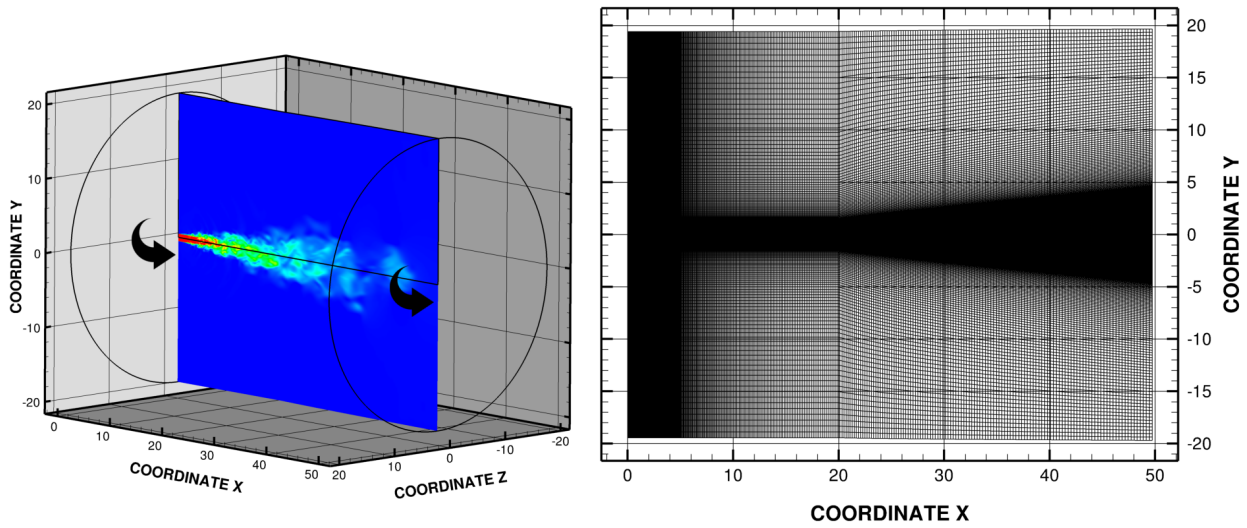

(a) Frontal view of the computational domain for the jet flow simulation

(b) 2-D view of the mesh generation.

Figura 2: Computational domain and mesh for a jet flow simulation

8. LARGE EDDY SIMULATION RESULTS

The present section is devoted to a study of a supersonic perfectly expanded jet flow. Results are compared with analytical, numerical and experimental data from the literature (Mendez *et al.*, 2010; Bridges and Wernet, 2008). The LES results using the Smagorinsky SGS turbulence closure (Smagorinsky, 1963) are discussed in the present work. Interested readers are referred to Refs. Junqueira-Junior (2016) for simulations using others subgrid scale models. The flow is characterized by an unheated perfectly expanded inlet jet with a Mach number of 1.4 at the domain entrance. Therefore, the pressure ratio, $PR = P_j/P_\infty$, and the temperature ratio, $TR = T_j/T_\infty$, between the jet exit and the ambient freestream are equal to one, $PR = 1$ and $TR = 1$. The time step used in the simulation is constant and equal to 2.5×10^{-4}. It has been nondimensionalized using the speed of sound of the jet at the inlet, a_j, and the jet diameter, D. The Reynolds number of the jet is $Re = 1.57 \times 10^6$. The radial and longitudinal dimensions of the smallest cell of the computational domain are given by $(\Delta \underline{r})_{min} = 0.002$ and $(\Delta \underline{x})_{min} = 0.0126$, respectively, again in dimensionless form. This cell is located in the shear layer of the jet, at the entrance of the computational domain. The number of points in the azimuthal direction is $N_\theta = 180$. The mesh domain is composed by 14.4 million points. The present mesh reproduces

well the main geometric characteristics of the reference grid (Mendez *et al.*, 2010).

Data are extracted, for the present study, after the simulation has run for 35 dimensionless time units. For the current jet exit velocity of $M_j = 1.4$, the simulation time represents approximately 4 flow-through times. One flow through time is the time for a particle to cross the entire domain from the jet entrance to the domain exit. The reader should remember that, as $TR = 1$ and $a_j = a_\infty$, the characteristic time in the present work is equal to that reported in the work of Mendez (Mendez *et al.*, 2010). The preliminary simulation is performed in order to achieve a statiscaly stationary flow. After the flow initialization process, the simulation is run for more 40 dimensionless times, in which data are extracted each 0.02 dimensionless time in order to calculate time averaged properties.

Figure 3 presents a lateral view of the time averaged axial component of velocity of the jet. The black solid line displays the potential core where the axial component of velocity reaches 95% of the axial jet velocity at the inlet, U_j. One of the most important characteristic of the jet is the length of the potential core. In the present work, the dimensionless potential core length is equal to 5.57, which is much lower than the numerical and experimental references displaying 8.35 and 9, respectively. However, the author decided to use this simulation as a benchmark for the DMD process presented in the next section. Figure 4 illustrates a comparison of profiles of averaged axial component of velocity at different positions to the inlet domain. The present results, blue line, are compared with the numerical simulation of Mendez *et al.* (2010), dashed line, and the experimental data of Bridges and Wernet, square points (Bridges and Wernet, 2008). One can notice that the current simulation correlates well with the references until $X = 2.5D$. The current study has presented to be very dissipative as the jet get closer to the output domain.

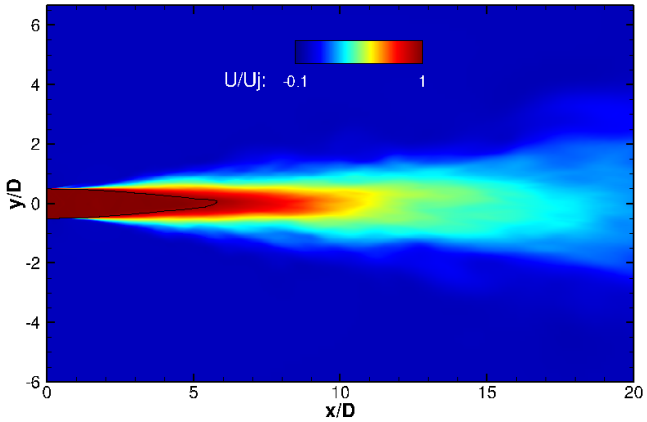

Figura 3: Lateral view of the averaged axial velocity component

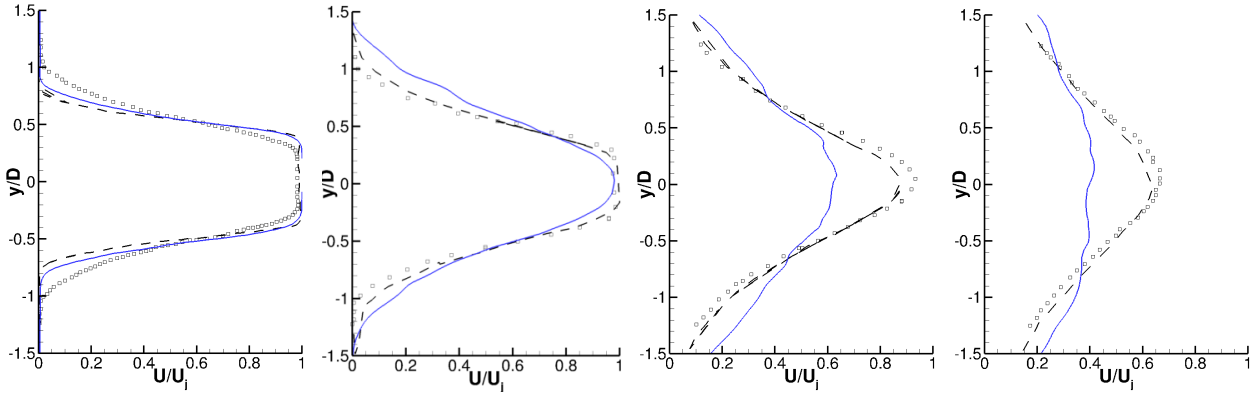

(a) X=0.5D (b) X=2.5D (c) X=5.0D (d) X=10D

Figura 4: Profiles of averaged axial component of velocity along the X coordinate

The evolution of the averaged axial component of velocity along the centerline and the lipline is illustrated in Fig. 5. As discussed before, one can observe that the simulation is over dissipative. The core of the jet is much smaller than the one that can be seen in the references. The 2nd-order scheme used in the present simulation is very dissipative for coarse meshes, such as the one used for this preliminary study. For furture work, the authors will use a very refined grid and more sophisticated SGS closures, such as the Vreman model (Vreman, 1995; Vremant *et al.*, 1995) and the dynamic Smagorinsky model (Moin *et al.*, 1991).

9. DYNAMIC MODE DECOMPOSITION RESULTS

We computed the streaming version (Hemati *et al.*, 2014) of the *Total-Least-Square* DMD algorithm (Hemati and Rowley, 2015) on a plane data extracted during large eddy simulations in its implicit form. This domain contains the jet

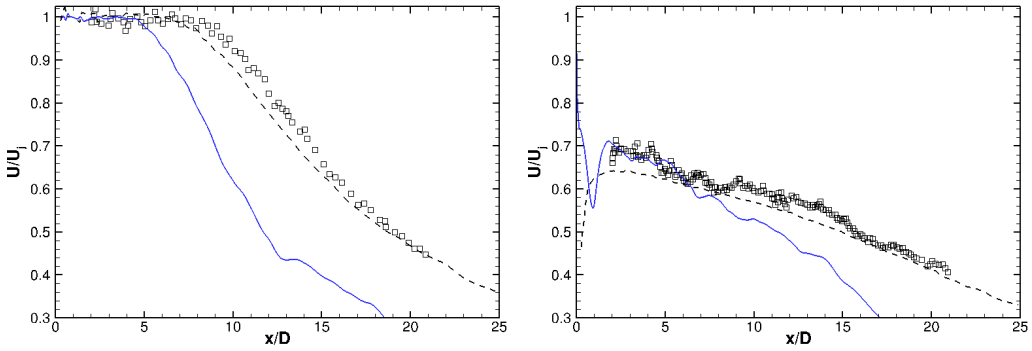

(a) Centerline (b) Lipline

Figura 5: Averaged axial component of velocity along the centerline and lipline

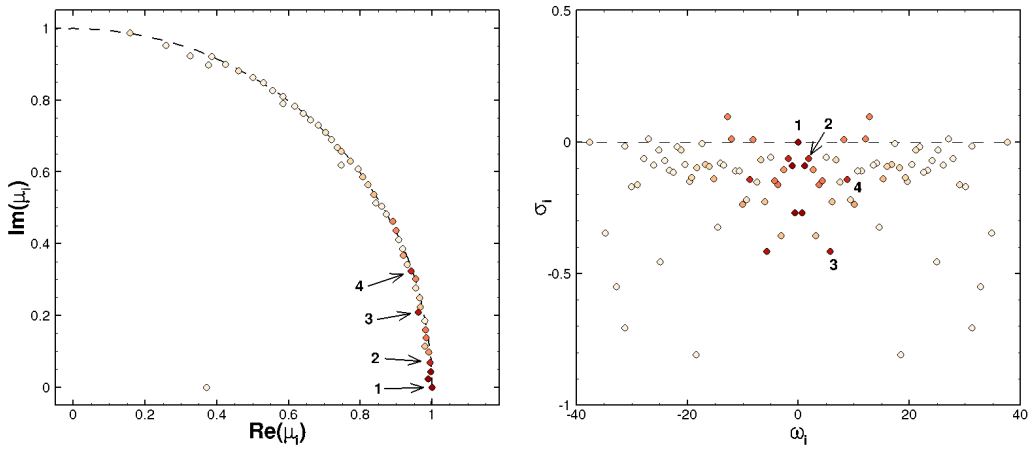

(a) (b)

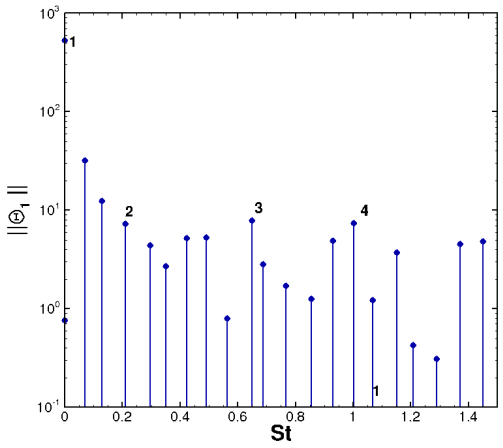

(c)

Figura 6: DMD spectra regarding (a) the eigenvalues μ of A, (b), the eigenvalues of the DMD modes λ and (c), the initial amplitude of the DMD modes $\|\theta_1\|$. In (a) and (b), the symbols are colored by the mode amplitude $\|\theta_1\|$.

entrance, the potential core and the near field of the jet. By doing so, the results should include the aerodynamic structures as well as the generated acoustic waves. We retained every 75th snapshot corresponding to a $\Delta t = 0.0325$. A number of 256 snapshots without substracting the mean has been considered. The streaming version of the DMD algorithm includes a compression step of the snapshots, allowing to choose the number r_0 ($r_0 < m - 1$) of computed spatial dynamic modes. For the present preliminary test, the authors chose $r_0 = 100$.

Figure 6 displays three different ways of reprensenting the DMD spectrum. In Fig. 6(a), the eigenvalues of the DMD linear operator A are shown. They are nearly all located on the unit circle suggesting that most of DMD modes are neutrally stable. The symbols are colored by the initial amplitude of the DMD modes $\|\theta_1\|$. The choice of this parameter to differentiate the modes comes from Eqs. (26) and (32). It has also been taken into account by Sayadi *et al.* (2013). Four modes displaying a high amplitude have been selected. Mode 1 is the most amplified mode corresponding to the mean flow, while the other modes are unsteady and possess a complex conjugate, symmetric with respect to the axis $\mathrm{Im}(\mu_i) = 0$. The growth rate of each mode σ_i is plotted versus the frequency ω_i in Fig. 6(b). It appears that the most unstable modes

($\sigma_i > 0$) are not necessarily the most amplified regarding $\|\theta_1\|$. Figure 6(c) represents the most amplified mode as a function of the strouhal number. The reader should note that the frequency of Mode 2 coincides with the experimental pressure peak observed by Bridges and Wernet (2008), and also by Jovanović *et al.* (2014).

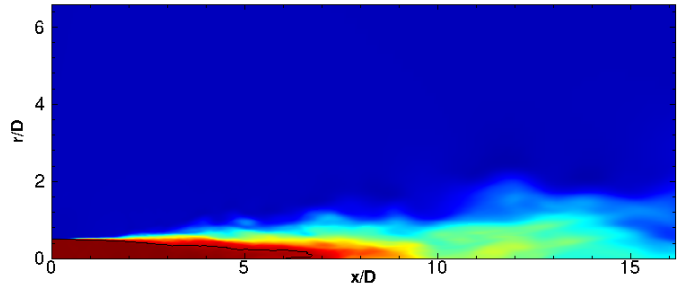

Figura 7: Averaged axial velocity component of the steady mode 1. The black line defines the potential core limits. Contours are the same as in Fig. 3.

The averaged axial velocity component of the steady mode 1 is shown in Fig. 7 using the same contoured of Fig. 3 displaying the LES mean flow. The mode has been reconstructed by multiplying with its initial amplitude $\|\theta_1\|$. A very good agreement is found regarding the potential core lentgh as well as the contour levels even if the sample rate and the number of snapshots are different.

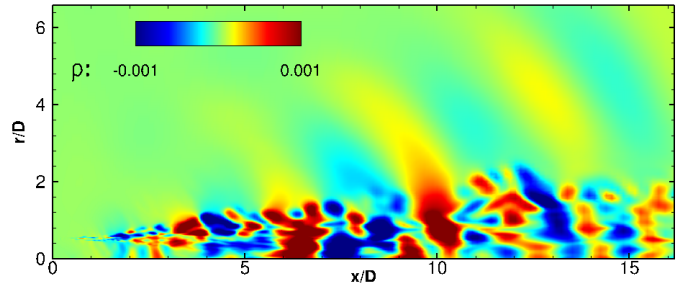

(a) Mode 2

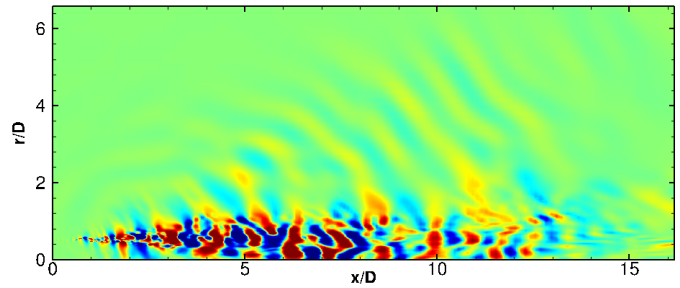

(b) Mode 3

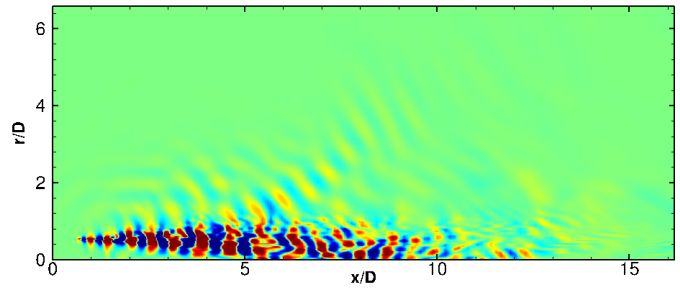

(c) Mode 4

Figura 8: Visualizations of the density contours for the real part of the mode 2 (a), the mode 3 (b) and the mode 4 (c).

Finally, real part of the modes 2, 3 and 4 are displayed in Fig. 8 through density contours. As expected, they all show vortical structures and acoustic waves with a wavelength depending on the DMD mode frequency. The higher ω_i is, the smaller are the vortical structures and the acoustic wavelength. Moreover, different authors argue the entrance of vortical structures at the end of the potential core influences the acoustic far field. This phenomenon could be analyzed by animating the mode, taking into account its imaginary part.

Future work will deal with the flow reconstruction considering the most relevant DMD modes. Similarly, acoustic predictions using the Ffowcs Williams and Hawkings analogy or the calculation of the acoustic sources will be performed

and compared with the large eddy simulation results.

10. CONCLUDING REMARKS

The present work is concerned with the study of aerodynamics and aeroacoustics of a perfectly expanded supersonic jet flow. A large eddy simulation (LES) formulation for compressible flows, based on the System I set of equations, is used. The Smagorinsky subgrid scale model is considered in the present effort. A 2nd-order centered method and a 5-stage, 2nd-order Runge-Kutta time integration scheme are used in the present study. Simulations are performed in a multiprocessor environment with the help of MPI protocols. In parallel, a dynamic mode decomposition algorithm was chosen to provide more information about the jet dynamics. Main axial velocity characteristics are extrated from the simulations and present a good agreement with the numerical and experimental reference work near the inlet region. However, this is not the case when the jet moves away from the domain entrance, the potential core length is clearly underestimated. Such behavior is expected since the low order numerical scheme used would require some quite extensive mesh refinements.

A preliminary DMD analysis has been performed by extracting a 2-D data plane from the LES results. Considering the high complexity of the supersonic jet flow, fairly good results are obtained regarding the references. In the future, dynamic mode decomposition of a three dimensional snapshots sequence will be performed. And the flow reconstruction based on the dominant extracted modes will allow the calculation of all the acoustic sources. It will then be interesting to analyze the contribution of each important mode in the directivity pattern.

11. ACKNOWLEDGEMENTS

The authors gratefully acknowledge the partial support for this research provided by Conselho Nacional de Desenvolvimento Científico e Tecnológico, CNPq, under the Research Grants No. 309985/2013-7, No. 400844/2014-1 and No. 443839/2014-0. The authors are also indebted to the partial financial support received from Fundação de Amparo à Pesquisa do Estado de São Paulo, FAPESP, under the Research Grants No. 2008/57866-1, No. 2013/07375-0 and No. 2013/21535-0.

12. REFERENCES

Abou-Taouk, A., Sadasivuni, S., Lörstad, D., Ghenadie, B. and Eriksson, L.E., 2015. "Cfd analysis and application of dynamic mode decomposition for resonant-mode identification and damping in an sgt-100 dle combustion system". In *Proceedings of the 7th European Combustion Meeting*.

Aupoix, B. and Cousteix, J., 1982. "Simple sub-grid strain models of isotrope homogeneous turbulence. in french: *Modèles Simples de Tensions de Sous-Maille en Turbulence Homogene Isotrope*". *La Recherche Aérospatiale*, Vol. 4, pp. 273–283.

Bagheri, S., 2013. "Koopman-mode decomposition of the cylinder wake". *Journal of Fluid Mechanics*, Vol. 726, pp. 596–623.

Berkooz, G., Holmes, P. and Lumley, J.L., 1993. "The proper orthogonal decomposition in the analysis of turbulent flows". *Annual review of fluid mechanics*, Vol. 25, No. 1, pp. 539–575.

Bigarella, E.D.V., 2002. *Three-Dimensional Turbulent Flow Over Aerospace Configurations*. M.Sc. Thesis, Instituto Tecnológico de Aeronáutica, São José dos Campos, SP, Brasil.

Bigarella, E.D.V., 2007. *Advanced Turbulence Modeling for Complex Aerospace Applications*. Ph.D. thesis, Instituto Tecnológico de Aeronáutica, São José dos Campos, SP, Brasil.

Bridges, J. and Wernet, M.P., 2008. "Turbulence associated with broadband shock noise in hot jets". *AIAA paper*, Vol. 2834, p. 2008.

Chen, K.K., Tu, J.H. and Rowley, C.W., 2012. "Variants of dynamic mode decomposition: boundary condition, koopman, and fourier analyses". *Journal of Nonlinear Science*, Vol. 22, No. 6, pp. 887–915.

Clark, R.A., Ferziger, J.Z. and Reynolds, W.C., 1979. "Evaluation of subgrid-scale models using an accurately simulated turbulent flow". *Journal of Fluid Mechanics*, Vol. 91, pp. 1–16. doi:0022-1 120/79/4207-6000.

Deardorff, J.W., 1970. "A numerical study of three-dimensional turbulent channel flow at large reynolds numbers". *Journal of Fluid Mechanics*, Vol. 41, part 2, pp. 453–480. doi:10.1017/S002211207900001X.

Garnier, E., Adams, N. and Sagaut, P., 2009. *Large Eddy Simulation for Compressible Flows*. Springer. doi:10.1007/978-90-481-2819-8.

Grilli, M., Schmid, P.J., Hickel, S. and Adams, N.A., 2012. "Analysis of unsteady behaviour in shockwave turbulent boundary layer interaction". *Journal of Fluid Mechanics*, Vol. 700, pp. 16–28.

Hemati, M.S. and Rowley, C.W., 2015. "De-biasing the dynamic mode decomposition for applied koopman spectral analysis". *arXiv preprint arXiv:1502.03854*.

Hemati, M.S., Williams, M.O. and Rowley, C.W., 2014. "Dynamic mode decomposition for large and streaming datasets". *Physics of Fluids (1994-present)*, Vol. 26, No. 11, p. 111701.

Jameson, A. and Mavriplis, D., 1986. "Finite volume solution of the two-dimensional euler equations on a regular triangular mesh". *AIAA Journal*, Vol. 24, No. 4, pp. 611–618.

Jameson, A., Schmidt, W. and Turkel, E., 1981. "Numerical solutions of the euler equations by finite volume methods

using runge-kutta time-stepping schemes". In AIAA Paper 81–1259*, Proceedings of the AIAA 14th Fluid and Plasma Dynamic Conference*. Palo Alto, Californa, USA.

Jourdain, G., Eriksson, L.E., Kim, S.H. and Sohn, C.H., 2013. "Application of dynamic mode decomposition to acoustic-modes identification and damping in a 3-dimensional chamber with baffled injectors". *Journal of Sound and Vibration*, Vol. 332, No. 18, pp. 4308–4323.

Jovanović, M.R., Schmid, P.J. and Nichols, J.W., 2014. "Sparsity-promoting dynamic mode decomposition". *Physics of Fluids (1994-present)*, Vol. 26, No. 2, p. 024103.

Junqueira-Junior, C., Yamouni, S. and Azevedo, J.L.F., 2015a. "On the development of large eddy simulation tools for compressible jet flow configurations". In *Proceedings of the 1st Pan-American Congress on Computational Mechanics (PANACM 2015) and XI Argentine Congress on Computational Mechanics (MECOM 2015)*. Buenos Aires, Argentina, pp. 1423–1434.

Junqueira-Junior, C., Yamouni, S., Azevedo, J.L.F. and Wolf, W.R., 2015b. "Large eddy simulations of supersonic jet flows for aeroacoustic applications". In AIAA Paper No. 2015-3306*, Proceedings of the 33rd AIAA Applied Aerodynamics Conference*. Dallas, TX.

Junqueira-Junior, C.A., 2016. *Development of a Parallel Solver for Large Eddy Simulation of Supersonic Jet Flow*. Ph.D. thesis, Instituto Tecnológico de Aeronáutica, São José dos Campos, SP, Brazil.

Lárusson, R., Hafsteinsson, H.E., Andersson, N. and Eriksson, L.E., 2014. "Investigation of supersonic jet flow using modal decomposition". In *20th AIAA/CEAS Aeroacoustics Conference*.

Lilly, D.K., 1967. "The representation of small-scale turbulence in numerical simulation experiments". In IBM Form No. 320-1951*, Proceedings of the IBM Scientific Computing Symposium on Environmental Sciences*. Yorktown Heights, N.Y., pp. 195–210.

Lilly, D.K., 1965. "On the computational stability of numerical solutions of time-dependent non-linear geophysical fluid dynamics problems". *Monthly Weather Review*, Vol. 93, No. 1, pp. 11–25. doi:10.1175/1520-0493(1965)093<0011:OTCSON>2.3.CO;2.

Long, L.N., Khan, M. and Sharp, H.T., 1991. "A Massively Parallel Three-Dimensional Euler/Navier-Stokes Method". *AIAA Journal*, Vol. 29, No. 5, pp. 657–666.

Lumley, J.L., 1970. *Stochastic tools in turbulence*. Academic Press.

Mendez, S., Shoeybi, M., Sharma, A., Ham, F.E., Lele, S.K. and Moin, P., 2010. "Large-eddy simulations of perfectly-expanded supersonic jets: Quality assessment and validation". In AIAA Paper No. 2010–0271. doi:10.2514/6.2010-271.

Meneveau, C., 1994. "Statistics of turbulence subgrid-scale stresses: Necessary conditions and experimental tests". *Physics of Fluids*, Vol. 6, No. 2, pp. 815–833. doi:10.1063/1.868320.

Meyers, J. and Sagaut, P., 2006. "On the model coefficients for the standard and the variational multi-scale smagorinsky model". *Journal of Fluid Mechanics*, Vol. 569, pp. 287–319. doi:10.1017/S0022112006002850.

Moin, P., Squires, K., Cabot, W. and Lee, S., 1991. "A dynamic subgrid-scale model for compressible turbulence and scalar transport". *Physics of Fluids A: Fluid Dynamics (1989-1993)*, Vol. 3, No. 11, pp. 2746–2757. doi:10.1063/1.858164.

O'Neil, J. and Meneveau, C., 1997. "Subgrid-scale stresses and their modelling in a turbulent plane wake". *Journal of Fluid Mechanics*, Vol. 349, pp. 253–293. doi:10.1017/S0022112097006885.

Rowley, C.W., Mezić, I., Bagheri, S., Schlatter, P. and Henningson, D.S., 2009. "Spectral analysis of nonlinear flows". *Journal of Fluid Mechanics*, Vol. 641, pp. 115–127.

Sagaut, P., 2002. *Large Eddy Simulation for Incompressible Flows*. Springer.

Sayadi, T., Schmid, P., Nichols, J. and Moin, P., 2013. "Dynamic mode decomposition of controlled h-and k-type transitions". Technical report, Tech. Rep., Annual Research Briefs.

Schmid, P.J., 2010. "Dynamic mode decomposition of numerical and experimental data". *Journal of Fluid Mechanics*, Vol. 656, pp. 5–28.

Schmid, P.J., 2011. "Application of the dynamic mode decomposition to experimental data". *Experiments in fluids*, Vol. 50, No. 4, pp. 1123–1130.

Schmid, P.J., Li, L., Juniper, M. and Pust, O., 2011. "Applications of the dynamic mode decomposition". *Theoretical and Computational Fluid Dynamics*, Vol. 25, No. 1-4, pp. 249–259.

Schmid, P.J., Violato, D. and Scarano, F., 2012. "Decomposition of time-resolved tomographic piv". *Experiments in fluids*, Vol. 52, No. 6, pp. 1567–1579.

Seena, A. and Sung, H.J., 2011. "Dynamic mode decomposition of turbulent cavity flows for self-sustained oscillations". *International Journal of Heat and Fluid Flow*, Vol. 32, No. 6, pp. 1098–1110.

Sirovich, L., 1987. "Turbulence and the dynamics of coherent structures. part i: Coherent structures". *Quarterly of applied mathematics*, Vol. 45, No. 3, pp. 561–571.

Smagorinsky, J., 1963. "General circulation experiments with the primitive equations: I. the basic experiment". *Monthly Weather Review*, Vol. 91, No. 3, pp. 99–164. doi:10.1175/1520-0493(1963)091<0099:GCEWTP>2.3.CO;2.

Stegeman, P., Soria, J. and Ooi, A., 2014. "Dynamic mode decomposition of near nozzle instabilities in large-eddy simulations of under-expanded circular jets." In *Australasian Fluid Mechanics Conference (Aleksandar Subic 08 December 2014 to 11 December 2014)*. RMIT University, pp. 1–4.

Tang, Z. and Jiang, N., 2012. "Dynamic mode decomposition of hairpin vortices generated by a hemisphere protuberance".

Science China Physics, Mechanics and Astronomy, Vol. 55, No. 1, pp. 118–124.

Tissot, G., Cordier, L., Benard, N. and Noack, B.R., 2013. "Dynamic mode decomposition of piv measurements for cylinder wake flow in turbulent regime". In *TSFP DIGITAL LIBRARY ONLINE*. Begel House Inc.

Tu, J.H., Rowley, C.W., Kutz, J.N. and Shang, J.K., 2014. "Spectral analysis of fluid flows using sub-nyquist-rate piv data". *Experiments in Fluids*, Vol. 55, No. 9, pp. 1–13.

Turkel, E. and Vatsa, V.N., 1994. "Effect of Artificial Viscosity on Three-Dimensional Flow Solutions". *AIAA Journal*, Vol. 32, No. 1, pp. 39–45. URL `http://doi.aiaa.org/10.2514/3.11948`.

Ulitsky, M. and Collins, L.R., 2000. "On constructing realizable, conservative mixed scalar equations using the eddy-damped quasi-normal markovian theory". *Journal of Fluid Mechanics*, Vol. 412, pp. 303–329. doi: 10.1017/S0022112000008363.

Vreman, A.W., 1995. *Direct and Large-Eddy Simulation of the Compressible Turbulent Mixing Layer*. Ph.D. thesis, Universiteit Twente.

Vremant, B., Geurts, B. and Kuerten, H., 1995. "A priori tests of large eddy simulation of the compressible plane mixing layer". *Journal of Engineering Mathematics*, Vol. 29, pp. 299–327.

Wan, Z.H., Zhou, L., Wang, B.F. and Sun, D.J., 2015. "Dynamic mode decomposition of forced spatially developed transitional jets". *European Journal of Mechanics-B/Fluids*, Vol. 51, pp. 16–26.

Williams, M., Rowley, C. and Kevrekidis, I., 2015. "A kernel-based approach to data-driven koopman spectral analysis". *arXiv preprint arXiv:1411.2260*.

Williams, M.O., Kevrekidis, I.G. and Rowley, C.W., 2014. "A data-driven approximation of the koopman operator: extending dynamic mode decomposition". *arXiv preprint arXiv:1408.4408*.

Wolf, W.R. and Lele, S.K., 2011. "Aeroacoustic integrals accelerated by fast multipole method". *AIAA Journal*, Vol. 49, No. 7, pp. 1466–1477. doi:10.2514/1.J050861.

Wynn, A., Pearson, D., Ganapathisubramani, B. and Goulart, P., 2013. "Optimal mode decomposition for unsteady flows". *Journal of Fluid Mechanics*, Vol. 733, pp. 473–503.

13. RESPONSIBILITY NOTICE

The following text, properly adapted to the number of authors, must be included in the last section of the paper: The author(s) is (are) the only responsible for the printed material included in this paper.